ELSEVIER

Biochimica et Biophysica Acta 1368 (1998) 184–200

BIOCHIMICA ET BIOPHYSICA ACTA
BBA

K^+-Dependence of electrogenic transport by the NaK–ATPase

T. Gropp [a], F. Cornelius [b], K. Fendler [a,*]

[a] *Max-Planck-Institut für Biophysik, Kennedyallee 70, 60596 Frankfurt, Germany*
[b] *Aarhus University, DK-8000 Aarhus, Denmark*

Received 1 May 1997; revised 30 June 1997; accepted 8 July 1997

Abstract

Charge translocation by the NaK–ATPase from shark rectal gland was measured by adsorption of proteoliposomes to a planar lipid membrane. The proteoliposomes were prepared by reconstitution of purified NaK–ATPase into liposomes consisting of *E. coli* lipids. The protein was activated by applying an ATP concentration jump produced by photolysis of a protected derivative of ATP, caged ATP. K^+ titrations were used to study the effect of K^+ on the charge translocation kinetics of the protein. The time-dependent currents obtained after activation of the enzyme with caged ATP were analyzed with a simplified Albers–Post model ($E_1 \overset{k_1}{\rightarrow} E_1ATP \overset{k_2}{\rightarrow} E_2P \overset{k_3}{\rightarrow} E_1$), taking into account the capacitive coupling of the protein to the measuring system. The results of the K^+ titrations show a strong dependence of the rate constant k_3 on the K^+ concentration at the extracellular side of the protein, indicating the K^+ activated dephosphorylation reaction. In contrast, k_1 and k_2 remained constant. The K^+ dependence of the rate k_3 could be well described with a K^+ binding model with two equivalent binding sites ($E_2P + 2K^+ \rightleftharpoons E_2P(K) + K^+ \rightleftharpoons E_2P(2K)$) followed by a rate limiting reaction ($E_2P(2K) \rightharpoonup E_1(2K)$). The half saturating K^+ concentration $K_{3,0.5}$ and the microscopic dissociation constant K_3 for the K^+ dependence of k_3 were 4.5 mM and 1.9 mM respectively. At saturating K^+ concentration the rate constant k_3 was approximately 100 s^{-1}. The relative amount of net charge transported during the Na^+ and the K^+ dependent reactions could be determined from the experiments. Our results suggest electroneutral K^+ translocation and do not support electrogenic K^+ binding in an extracellular access channel. This is compatible with a model where 2 negative charges are cotransported with $3Na^+$ and $2K^+$ ions. Error analysis gives an upper limit of 20% charge transported during K^+ translocation or during electrogenic K^+ binding in a presumptive access channel compared to Na^+ translocation. © 1998 Elsevier Science B.V.

Keywords: NaK–ATPase; K^+ translocation; Electrogenic; Bilayer; Liposome

1. Introduction

One of the most thoroughly investigated enzymes of the class of ion translocating proteins is the NaK–ATPase. This protein transports $3Na^+$ ions out of the cell and imports $2K^+$ ions into the cell, all at the expense of energy provided by the hydrolysis of ATP. Na^+ transport takes place during the formation of the phosphoenzyme E_2P while K^+ transport is correlated with the decay of E_2P and the formation of the ground state E_1. This sequential transport model is supported by a large bulk of experimental evidence (for a review, see [1]).

The formation of the phosphoenzyme and its decay can be followed by time-resolved rapid mixing meth-

* Corresponding author. Fax: +49 69 6303-305; E-mail: fendler@kennedy.biophys.mpg.de

PII S0005-2736(97)00162-4

ods [2,3]. This yields rate constants for the partial reactions of the reaction cycle. A correlation of the reaction cycle and charge transport was obtained by comparing rapid mixing phosphorylation measurements and electrical experiments on lipid bilayers [4].

The translocation of Na^+ during the conformational transition $E_1P \rightarrow E_2P$ has been considered as an electrogenic reaction step as shown in several publications [5–7]. But also extracellular Na^+ deocclusion [8,9] and cytoplasmic Na^+ binding were proposed to be electrogenic [10,11]

In contrast to Na^+ transport, K^+ transport was suggested to be electroneutral [12,13]. The model proposed in this context was the cotransport of two negative charges with the two K^+ ions. However, extracellular binding of K^+ was found to be electrogenic [14,8,15].

In the rapid mixing phosphorylation measurements the decay of E_2P was found to be extremely slow in the absence of K^+ [2,16] ($k \approx 0.4\,s^{-1}$) while with K^+ the rate constant for dephosphorylation reaches values up to $600\,s^{-1}$. These values are well within the reach of time-resolved electrical measurements. However, analysis of current measurements performed on lipid bilayers in the presence of K^+ did not yield an exponential component related to K^+ transport [17,6].

In the presence of conflicting reports about the electrical nature of K^+ transport, we evaluated the electrical signal at various K^+ concentrations on the basis of a simple model. The differential equations describing the kinetic model were directly fitted to the data. As a second approach, we used the analytical solutions. The analysis shows that K^+ translocation is electroneutral within the limits of error.

Values reported for the K^+ dissociation constants of the phosphoenzyme E_2P range from 0.2 to 10 mM. The great variation of results can be partly explained by the fact that some of these measurements were performed under conditions where subsequent rate limiting reactions lead to different apparent dissociation constants for K^+. But, enzyme sources and isoforms may also contribute to differences. To obtain a realistic value for the intrinsic K^+ dissociation constant it is essential to consider only that part of the reaction cycle that is related to K^+ binding. However, the study of equilibrium binding of K^+ to the E_2P form is impossible since its K^+ bound form $E_2P(2K)$ is inherently instable. In this publication, we determine the rate constant for the K^+ dependent part of the reaction cycle at various K^+ concentrations. These results yield a microscopic dissociation constant for the reaction $E_2P + 2K^+ \rightleftharpoons E_2P(K) + K^+ \rightleftharpoons E_2P(2K) \rightarrow E_1$. This is as close as we can get to the equilibrium K^+ dissociation constant of E_2P and represents a lower limit for it.

2. Materials and methods

2.1. Preparation and reconstitution of the NaK–ATPase

NaK–ATPase was prepared from shark rectal glands according to Esmann et al. [18]. The purification of the protein was carried out by B. Kelety (Max-Planck-Institut für Biophysik, Frankfurt). The solution of microsomal membranes contained $4\,mg\,ml^{-1}$ protein.

The reconstitution of the NaK–ATPase into the phospholipid vesicles was similar to a method published by Cornelius [19]. The lipid that was used for vesicle preparation consisted of at least 50% phosphatidyl–ethanolamine and was taken from the plasma membrane of *E. coli* bacteria (Sigma). The lipid was further purified by an acetone/ether extraction.

The proteoliposomes were prepared as follows. 10 mg of the appropriate lipid in chloroform was transferred to a test tube with a ground glass stopper. In order to obtain a thin lipid film, the $CHCl_3$ was evaporated under N_2 while rotating the test tube. The residual solvent was then removed under vacuum for 10 min. 1 ml of buffer solution (130 mM NaCl, 3 mM $MgCl_2$, 25 mM imidazole, pH 6.2) plus 1 mg $C_{12}E_8$ was added and incubated for 1 h at room temperature. This was followed by sonication until the solution was transparent. The solution was stored on ice. Now, 17 μl of a 2.08 M NaCl solution and 33 μl of 130 mM NaCl plus 4 mg $C_{12}E_8$ solution were added to 250 μl of the protein containing suspension (= 1 mg protein). Solubilization of the protein occurred instantaneously. The suspension was centrifuged for 15 min at $100\,000 \times g$ to remove the nonsolubilized material and kept on ice. The solubilized lipid and the protein were mixed and incubated on ice for 15 min. The $C_{12}E_8$ was removed by adding Biobeads [20].

For this purpose, Biobeads were prewashed with a buffer solution and 400 mg were added to the suspension. The suspension was stirred for 8–10 h at 4°C. The Biobeads were then replaced by 200 mg of new Biobeads and the suspension was stirred for 1 h at room temperature. After removing the Biobeads, the suspension was centrifuged for 5 min at $10\,000 \times g$ and finally frozen in liquid N_2 as 50 μl samples. The protein concentration in the suspension was calculated to be approximately 0.8 mg ml^{-1}.

2.2. BLM measurements

Pump currents of the NaK–ATPase were measured by adsorption of the proteoliposomes to a black lipid membrane (BLM) in the same way as described elsewhere for membrane fragments (see Fig. 1) [17,21]. The BLM is formed in a teflon cuvette consisting of two compartments, while each compartment has a volume of 1.5 ml. Two buffer solutions were used for the experiments: (1) 130 mM NaCl, 3 mM $MgCl_2$, 1 mM DTT, 25 mM imidazole, pH 6.2; (2) 40 mM NaCl, 3 mM $MgCl_2$, 90 mM choline chloride, 1 mM DTT, 25 mM imidazole, pH 6.2. The temperature was kept at 24°C.

The signal was amplified (10^9-fold), filtered (1 kHz with a first-order low pass filter) and recorded with a digital oscilloscope.

For the BLM experiments 15–20 μl of the protein containing suspension were sonicated for 5–10 s and added to one compartment of the cuvette. Then, 300 μM of caged ATP was added to the suspension. Under stirring, the adsorption of the liposomes to the BLM took approximately 90 min, after which time saturation of the peak current was attained.

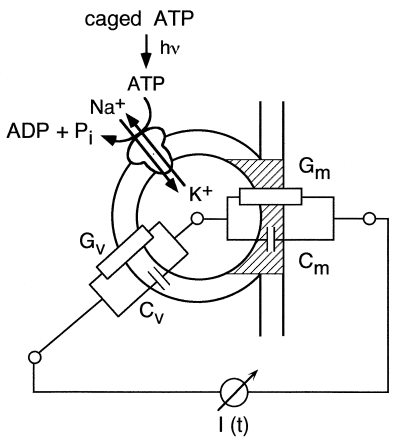

Fig. 1. Schematic depiction of a liposome adsorbed to a planar lipid bilayer and the corresponding equivalent circuit: G_v = conductance of the liposomes; C_v = capacitance of the liposomes; G_m = conductance of the BLM; C_m = capacitance of the BLM; $I(t)$ = measured current.

The caged ATP was photolyzed by a UV light pulse of an excimer laser (wavelength: 308 nm, pulse duration: 10 ns), that was focused onto the BLM. The average radiant exposure on the BLM surface was 120 mJ cm^{-2}, which corresponds to a release of 21% ATP from caged ATP. At pH 6.2, the release of ATP from caged ATP occurs rapidly ($\tau \approx 2.5$ ms at pH 6.2, 3 mM Mg^{2+} and 24°C; [22,23]).

Between two flashes there was a waiting period of 10 min. During that time the suspension was stirred so that the remaining ATP could be diluted and finally hydrolyzed by the NaK–ATPase remaining in the solution.

2.3. Analysis of the electrical signals on the basis of a kinetic model

The evaluation of the data was based on a kinetic model which is a simplified Albers–Post mechanism:

$$E_1 \overset{k_1}{\rightarrow} E_1ATP \overset{k_2}{\rightarrow} E_2P \overset{k_3}{\rightarrow} E_1. \quad (1)$$

This is a minimal model and was chosen to yield the same number of relaxation time as experimentally observed (2 relaxation times plus the system time constant). The first step of the reaction cycle includes the ATP binding and the exchange of ATP with caged ATP at the binding site, the second step the phosphorylation $E_1 \rightarrow E_1P$ and the conformational transition $E_1P \rightarrow E_2P$, and the third step the dephosphorylation $E_2P \rightarrow E_2$ and the conformational transition $E_2 \rightarrow E_1$. Na^+ and K^+ are translocated in the $E_1P \rightarrow E_2P$ and the $E_2 \rightarrow E_1$ conformational transition, respectively.

The differential equations describing the kinetic model (see Eqs. (10)–(12) in Appendix A) were directly fitted to the data (see Appendix C) with the fit program SCIENTIST (MicroMath Scientific Software). The program uses a modified Powell algorithm for least squares fitting. Assuming only electrogenic Na^+ transport (k_2) the following model function for the measured current $I(t)$ was used:

$$I(t) = sc(k_2 y_2 - k_0 u_m). \quad (2)$$

Here, y_2 is the concentration of the enzyme in the

E_1ATP state and u_m is the voltage across the bilayer generated by the ion pump. Both are calculated from the differential equations given in Appendix A and Appendix C. As a set of parameters k_1, k_2, k_3, the reciprocal system time constant k_0 and a scaling factor *sc* were used. The scaling factor *sc* is proportional to the number of contributing ion pumps and the amount of charge transported in the electrogenic step.

As shown in Appendix A, an analytical solution of the kinetic model is also possible. Three different solutions are found, depending on the choice of parameters k_i. As a result of this, there is no unambiguous analytical fitting function that can be used to evaluate the data. Therefore, the results of the fit with differential equations were used to chose the appropriate analytical solution (Eq. (26) or Eq. (27) in Appendix B). The corresponding model function (Eq. (30) or Eq. (31) in Appendix C) was then fitted to the data.

For the determination of the electrogenicity of the Na^+ and K^+ dependent steps in the reaction cycle, the reactions represented by k_2 and k_3 were assumed to be both electrogenic but to a different extent and with opposite polarity. For this purpose, we introduced the concentration of the intermediate (y_3) preceding the K^+ transport step into Eq. (29) and varied the number of negative charges n_-, that are cotransported together with the $3Na^+$ and the $2K^+$ ions in the two reaction steps:

$$I = sc\left[(3 - n_-)k_2 y_2 - (2 - n_-)k_3 y_3 - k_0 u_m\right]. \quad (3)$$

The mechanistic basis of this model is that the n_- negative charges are located at the cation binding sites and are fixed to the protein. These charges could be part of the cation binding sites[12,5].

Using Eq. (3) we determined the reduced least square sum $\chi^2_{red} = \sum_{i=1}^{n}(<I_i> - I_i)^2/(\sigma^2(m-n))$ for different values of n_-. $<I_i>$ and I_i are the calculated and the measured current at time t_i, respectively, n and m are the number of data points and parameters, respectively. The standard deviation σ of the data points was determined from a base line sampled before the UV flash. For the fit procedure in this case, we used the program MLAB (Civilized Software).

As shown in the equivalent circuit of the liposomes adsorbed to the planar bilayer (see Fig. 1), the ion pumps are capacitively coupled to the electrical circuit. Therefore, an additional differential equation describing the capacitive coupling had to be introduced (see Appendix C; [21]). This results in an additional exponential component with the system time constant τ_0 in the analytical fitting function. In the absence of ionophores, the conductivity of the BLM is negligible, so that the system time constant is $\tau_0 \approx \frac{C_m + C_v}{G_v}$.

3. Results

3.1. Characterization of the proteoliposomes

The size of the liposomes was determined by inelastic light scattering. The peak of the size distribution was at a diameter of approximately 140 nm. From the weight ratio protein:lipid (1:10), the average number of pumps reconstituted into one liposome was calculated to be approximately 80, assuming the following values: liposome diameter 140 nm, membrane thickness 4 nm, lipid density 1 g cm^{-3}, molecular mass of NaK–ATPase 148 000 $\times$ g mol^{-1}. The amount of active inside out oriented NaK–ATPase is probably significantly lower, because a certain amount of protein is either not incorporated into the liposomes, not active, right side out oriented or not oriented at all. Cornelius [24] determined a ratio of 65:15:20 for right side out:inside out:non oriented. Therefore, it has to be assumed that only 10–20% of the protein is reconstituted inside out and can give vectorial ion-transport activated by ATP.

Using the fluorescent potential sensitive dye Oxonol VI [25–27], we verified the functional reconstitution of NaK–ATPase into liposomes. After addition of ATP to the solution, an increase of the flourescence intensity was observed (signals not shown). This corresponds to the build-up of a positive potential inside the liposomes.

3.2. Transient current signals at different K^+ concentrations

The Na^+/K^+ exchange is the physiological transport mode of the NaK–ATPase. Since ATP cannot permeate the liposome membrane, only the inside-out

oriented molecules are activated by an ATP concentration jump and can pump Na^+ into and K^+ out of the liposomes. A constant Na^+ and K^+ concentration inside the liposomes was ensured by the addition of 5–10 μM monensin to the solution. Monensin exchanges Na^+ and K^+ against H^+ electroneutrally. The solution was buffered with 25 mM imidazole, so that no pH gradient could be generated.

In order to investigate the effect of K^+ on the charge translocation of the NaK–ATPase, the K^+ concentration was gradually increased from 0 up to 20 mM within each experiment (see Fig. 2). The experiments were carried out at two different Na^+ concentrations of the buffer solution (130 and 40 mM) to detect a possible effect of the Na^+ concentration on the K^+ affinity. Both concentrations are high enough to saturate the cytoplasmic Na^+ binding site. The ionic strength was kept approximately constant by adding 90 mM choline chloride to the 40 mM Na^+ buffer.

The transient current signal starts with a fast peak with a negative amplitude at $t = 0$–2 ms (Fig. 2). This is a light artefact caused by the illumination of the membrane and by the photolytic reaction caged ATP → ATP [6,28]. Therefore, only data sampled at $t > 1$ ms were used for the analysis. At $[K^+] = 0$ the data were fitted from $t = 0$ to $t = 700$ ms, so that the system time constant τ_0 could be obtained properly. Except for $[K^+] = 0$, the data were evaluated from $t = 2$ ms to $t = 200$ ms, which was found to be a sufficient time range for the investigated properties of the NaK–ATPase. Evaluations of a longer time range afforded an additional exponential function, which was difficult to interpret in terms of properties of the protein. Most likely, concentration effects inside and outside the liposomes have to be considered in this case. These effects were not taken into account for the evaluation of the data.

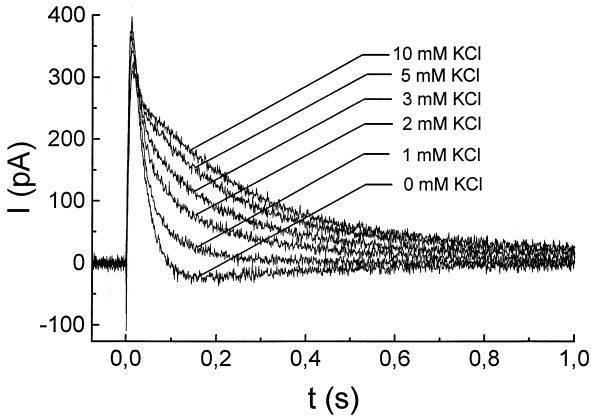

Fig. 2. Transient currents of NaK–ATPase at different K^+-concentrations. Buffer solution: 130 mM NaCl, 3 mM $MgCl_2$, 1 mM DTT, 25 mM imidazole, pH 6.2, 300 μM cATP, 5 μM monensin; temperature 24°C; ATP release $\eta = 0.17$.

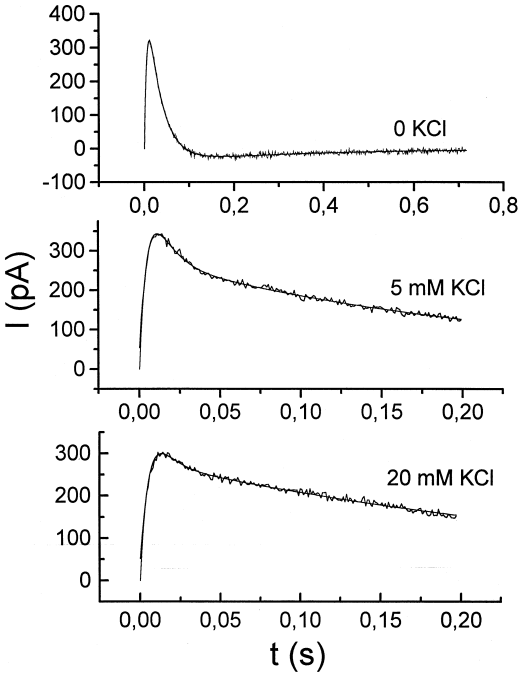

Fig. 3. Differential equation fit of NaK–ATPase signal with 0, 5, and 20 mM KCl in the buffer solution (conditions, see Fig. 2; parameter values, see Fig. 4).

In the absence of K^+, the transient signal is characterized by three phases: a rapid rise ($k_2 \approx 200\,s^{-1}$), a slower decay ($k_1 \approx 30\,s^{-1}$) and a very slow component with a negative amplitude ($k_0^{-1} \approx 330$ ms). After addition of K^+ to the buffer solution, the slow phase with the negative amplitude turns into a phase with positive amplitude. With increasing $[K^+]$ the stationary pumping increases the amplitude of the slowest decaying phase (see Fig. 2).

In Fig. 3, three typical transient signals at different K^+ concentrations are depicted and the corresponding differential equation fit is shown. As will be shown below only Na^+ transport $E_1ATP \rightarrow E_2P$ is electrogenic. As a consequence, the model function used in these fits was (Eq. (1)) which corresponds to

an electroneutral K^+ transport. Good quality fits were obtained using this model function. The parameters obtained are summarized in Fig. 4(A) and (B).

As shown in Fig. 4(A), a clear dependence of the reaction rate constant k_3 on the K^+ concentration was found on the one hand, whereas on the other hand k_1 and k_2 remained constant at different K^+ concentrations. Interestingly, also the scaling parameter *sc* was approximately the same in the presence and absence of K^+ indicating that the amount of charge that is translocated in one reaction cycle does not depend on K^+. This experiment was carried out at 130 mM Na^+. The same result was found for a Na^+ concentration of 40 mM in the buffer solution (see Fig. 4(B)).

3.3. K^+ dependence of k_3

The K^+ dependence of the reaction rate constant k_3 was evaluated on the basis of a two-step binding model for K^+ with two independent equivalent binding sites. A fitting function derived from a simple

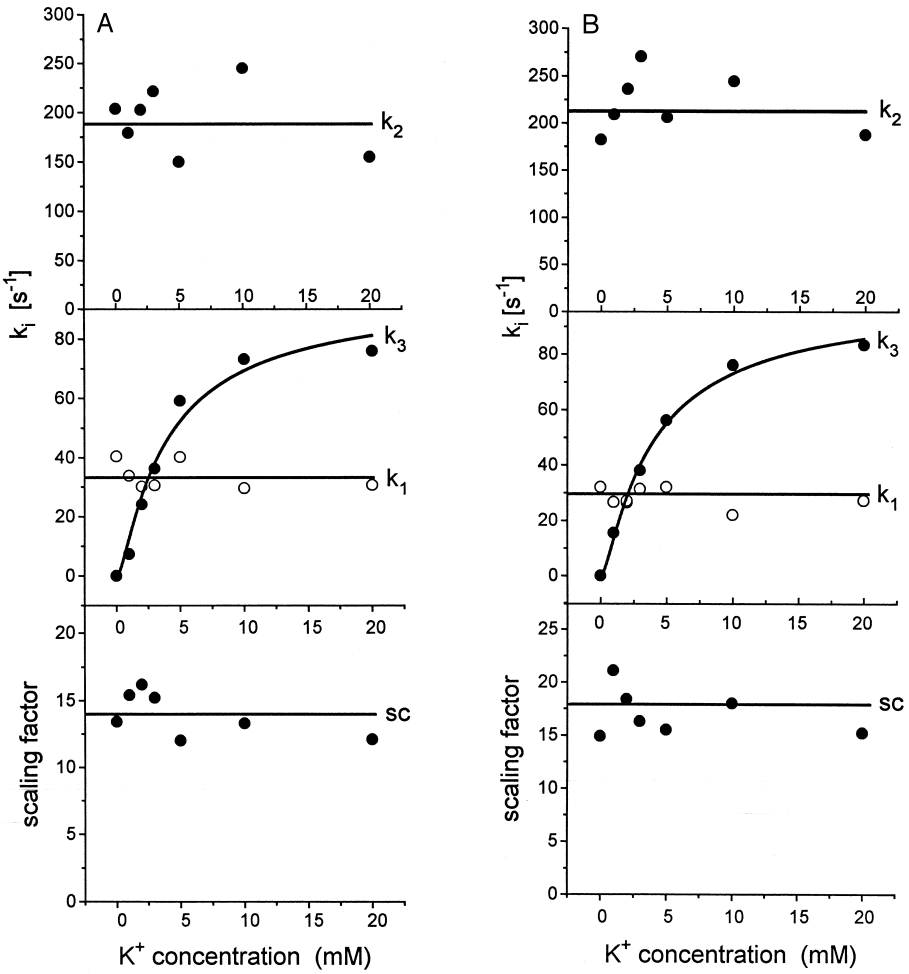

Fig. 4. (A) Parameter values of differential equation fits for the experiment shown in Fig. 2. The K^+ dependence of k_3 is evaluated with the fitting function (5). Apparent dissociation constant $K_3 = 1.78$ mM, half saturating concentration $K_{3,0.5} = 4.29$ mM (Experiment 1, Table 1). (B) Parameter values of differential equation fits for an experiment with 40 mM Na^+ concentration. Apparent dissociation constant $K_3 = 1.78$ mM, half saturating concentration $K_{3,0.5} = 4.29$ mM (Experiment 3, Table 1). Buffer solution: 40 mM NaCl, 3 mM $MgCl_2$, 90 mM cholinechloride, 1 mM DTT, 25 mM imidazole, pH 6.2, 10 μM monensin, 300 μM cATP; temperature 24°C; ATP release $\eta = 0.24$.

one-step binding model was found to be insufficient to properly fit the sigmoidally shaped K^+ dependence.

$$E_2P + 2K^+ \rightleftharpoons E_2P(K) + K^+ \rightleftharpoons E_2P(2K) \overset{k_{3,max}}{\rightarrow} E_1. \quad (4)$$

Since the K^+ binding is much faster than the following step in the reaction scheme, an equilibrium of the first three intermediates (E_2P, $E_2P(K)$, $E_2P(2K)$) can be assumed. This results in an effective reaction rate constant k_3

$$k_3 = k_{3,max} \frac{c^2}{K_3^2 + 2K_3c + c^2}. \quad (5)$$

K_3 is the microscopic dissociation constant for a single binding site [29] and c is the K^+ concentration. The half saturating concentration is given by

$$K_{3,0.5} = (1 + \sqrt{2})K_3. \quad (6)$$

This model yields an effective K^+ dependent rate constant k_3 and a microscopic dissociation constant for the two equivalent binding sites. $k_{3,max}$ is the value of k_3 at saturating K^+ concentration.

In Table 1, the microscopic dissociation constant, the half saturating concentration and the maximum values of k_3 are listed for experiments at the two different Na^+ concentrations. Since the fitting procedure with differential equations is extremely time-consuming, only the data of four experiments were analyzed. The values given in Table 1 are independent of the Na^+ concentration. This rules out competitive inhibition of K^+ binding by Na^+ in this concentration range.

To verify the K^+ dependence of k_3, fits with the corresponding analytical solution of the differential equations (see Section 2) were carried out for the data of Experiment 1. Here, the set of fit parameters was different from the fit with differential equations (see Appendix C). The parameters τ_2^{-1} and ω_1 can be expressed as functions of all three reaction rate constants k_1, k_2 and k_3 (see Appendix A). The choice for the appropriate fitting function ($d > 0$ or $d < 0$) was made on the basis of the differential equation fit results. From the parameter values τ_2^{-1} and ω_1 (see Table 2 and Appendix C), the reaction rate constant k_3 could be calculated (see Appendix A, Eqs. (14) and (22)), assuming k_1 and k_2 to be constant at different K^+ concentrations. From measurements with $[K^+] = 0$, the reaction rate constants $k_1 = \tau_2^{-1}$ and $k_2 = \tau_1^{-1}$ (since $k_3 \approx 0$) were determined (33 and 152 s^{-1}). In Table 2, the values for τ_2^{-1}, ω_1 and k_3 are shown for each K^+ concentration (data from Experiment). The resulting k_3 values (Table 2) have approximately the same K^+ dependence as the k_3 values from the differential equation fits (Fig. 4(A)). Therefore, the fits with analytical functions are considered as a verification of the differential equation fit method in order to support the consistency of the applied model.

Furthermore, the results from the differential equation fits clearly show that only at $[K^+] = 0$–2 mM the signal of the NaK–ATPase can be described by exponential functions, whereas at higher K^+ concentrations, it is described by a damped sine function. However, the damping factor is extremely high, so that the resulting curve is similar to a curve described by exponential functions. Since there is not a very slow step in the reaction cycle, it is not possible to assign different phases of the signal to particular time constants as it is in the case of pure Na^+/Na^+ exchange. Rather, the observed relaxation time constants of the Na^+/K^+ exchange are functions of k_1, k_2 and k_3.

Table 1
Dissociation constant K_3, half saturating value $K_{3,0.5}$ and maximum reaction rate constant $k_{3,max}$ for the K^+ dependence of k_3 at 130 and 40 mM Na^+ concentration in the buffer solution

Experiment No.	$[Na^+]$	K_3	$K_{3,0.5}$	$k_{3,max}$
1	130 mM	1.78 mM	4.29 mM	101.3 s^{-1}
2	130 mM	2.03 mM	4.89 mM	124.4 s^{-1}
3	40 mM	1.78 mM	4.29 mM	96.3 s^{-1}
4	40 mM	1.85 mM	4.46 mM	122.4 s^{-1}

Table 2
Calculated values of the reaction rate constant k_3 from the reciprocal time constants (τ_2^{-1} and ω_1) of the analytical fits (conditions, see Fig. 2)

$[K^+]$ (mM)	0	1	2	3	5	10	20
τ_2^{-1} (s^{-1})	33.7	50.5	83.7	–	–	–	–
ω_1 (s^{-1})	–	–	–	117.6	122.4	132.2	128.8
k_3 (s^{-1})	0	12	33	48	58	78	72

3.4. Stationary current signals at different K^+ concentrations

Stationary currents could be measured after addition of 10 μM 1799, a protonophore, which, in combination with monensin, induces a specific conductivity of approximately 30 $\mu S\,cm^{-2}$ across the planar lipid membrane. This value was reached after 90 min of incubation with 1799 and remained constant from then on.

Stationary currents were measured for the same K^+ concentrations as in the case of transient measurements. In Fig. 5, the stationary currents for a K^+ concentration ranging from 0 to 3 mM are depicted. The stationary currents correspond directly to the pump current $I_p(t)$ weighted with a factor $G_m/(G_v + G_m)$.

For the evaluation of the K^+ dependence of the stationary current amplitude (Fig. 6), the same K^+ binding model (Eqs. (4)–(6)) as for the transient current signals was used (see Fig. 6) except that the turnover rate constants k_t (which is proportional to the stationary current I_∞) and $k_{t,max}$ replace k_3 and $k_{3,max}$, respectively in Eq. (5). This fitting function can be used because the same K^+ binding process is determining the apparent K^+ dependence of the stationary current. We only have to assume that all the other processes in the reaction cycle are not K^+ dependent. This assumption is supported by the fact that k_1 and k_2 remain constant at different K^+ concentrations (see Fig. 4(A) and (B)).

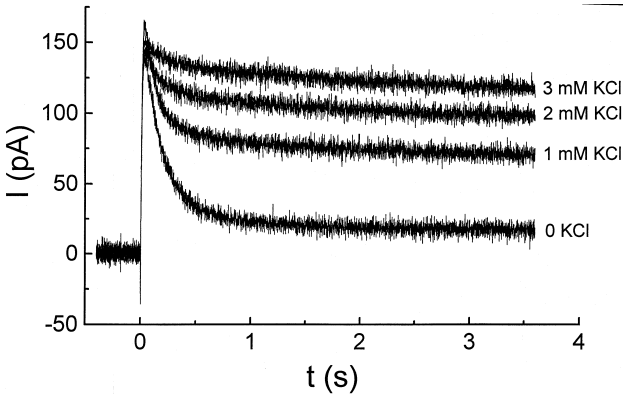

Fig. 5. Stationary current at 0, 1, 2, and 3 mM KCl. Buffer solution: 130 mM NaCl, 3 mM $MgCl_2$, 1 mM DTT, 25 mM imidazole, pH 6.2, 5 μM monensin, 10 μM 1799, 300 μM cATP; temperature 24°C; ATP release $\eta = 0.15$; conductivity $G = 30\ \mu S/cm^2$.

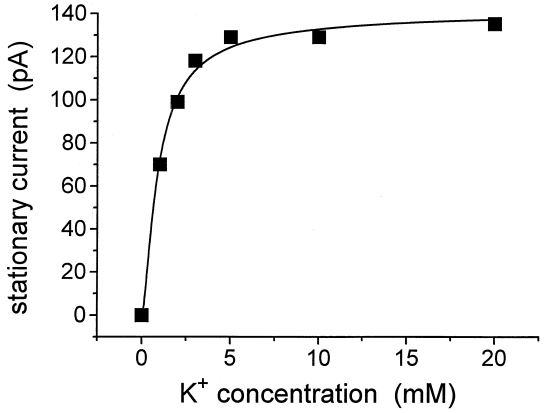

Fig. 6. Stationary current amplitudes at different K^+ concentrations (conditions, see Fig. 5). Apparent dissociation constant $K_t = 0.39$ mM, half saturating value $K_{t,0.5} = 0.95$ mM.

The fit of the K^+ dependence of the stationary currents yielded a half saturating concentration $K_{t,0.5}$ of approximately 0.95 mM and a microscopic dissociation constant $K_t = 0.39$ mM. This has to be compared to the half saturating concentration determined from the transient currents of $K_{3,0.5} \approx 4.5$ mM. The difference is due to the fact that different parts of the reaction cycle are involved in determining these values. In the discussion, it will be shown, that the two results are consistent.

3.5. Two electrogenic steps in the reaction cycle?

Both, Na^+ translocation (k_2) as well as K^+ translocation (k_3) are possible candidates for electrogenic steps while ATP-binding is electroneutral [6]. As outlined in the Section 2, the extent of electrogenicity of the two translocation steps can be described by the number n_- of cotransported negative charges. Therefore, we tested a model with different values of n_-. Signals recorded at $[K^+] = 0$, 5 and 20 mM, were fitted simultaneously with different values of n_-. In each of these fits n_- was kept constant at a value of 1, 1.5, 1.75, 2, 2.25, 2.5 or 2.75. The reaction rate constants k_1 and k_2 were assumed not to depend on the K^+ concentration and taken from experiments at $[K^+] = 0$. Variable fit parameters were *sc*, k_3 and k_0. While *sc* was only one parameter for all three K^+ concentrations, k_3 and k_0 could be

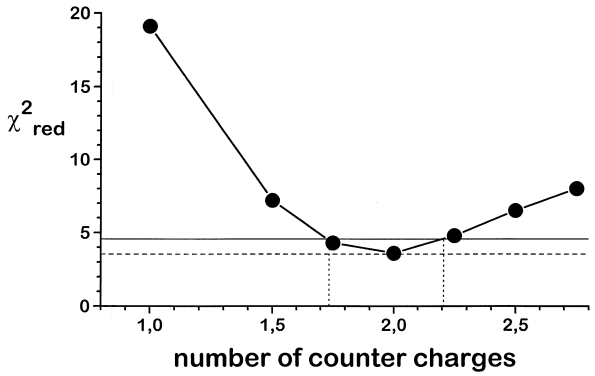

Fig. 7. Reduced sum of squared deviations (χ^2_{red}) over number of counter charges n_- for the Na^+ and K^+ transport. $[K^+]=0$, 5, 20 mM, data from Experiment 1.

determined independently for the different K^+ concentrations. The reduced sum of squares χ^2_{red} determined for the different values of n_- are depicted in Fig. 7. The error limits of a parameter are given by its value at the point where χ^2_{red} has increased by 1 from its optimal value [30]. The optimal level $\chi^2_{red}(0)$ and the increased values $\chi^2_{red}(0)+1$ (labeled σ and corresponding to a confidence level of 68%) are included in the figure. From the figure, we obtain a value of $n_-=2.0(+0.2, -0.27)$ countercharges. This corresponds to the transport of 1 net charge during Na^+ transport and to an electroneutral K^+ transport. Particularly, the application of the model function (2) for evaluation of the K^+ dependence as applied above is justified by this finding.

4. Discussion

4.1. The NaK − ATPase signal at different K^+ concentrations

The transient current signal at $[K^+]=0$ is characterized by three phases, which were investigated thoroughly in the past [28]. The fast rising phase is determined by three processes in the same time range: ATP release from caged ATP, phosphorylation of the NaK–ATPase and the conformational transition $E_1P \rightarrow E_2P$. The slower decay corresponds to the ATP binding and the exchange with caged ATP. The slowest component with a negative amplitude represents the system time constant ($\tau_0=k_0^{-1}$). The results of the experiments presented in this publication are in good agreement with earlier investigations with membrane fragments from eel electric organ, taking into account the parameters of photolytic ATP release of the corresponding experiments.

At $[K^+]=0$, the reaction rate constant k_3 is approximately $0.4\,s^{-1}$, which is the rate limiting reaction under these conditions. This is in fair agreement with a rate constant of $0.3\,s^{-1}$ at 10°C for the dephosphorylation reaction in the absence of K^+(Na^+/Na^+ exchange) determined earlier [31,32]. After the addition of K^+ to the buffer solution, the pump generates a stationary pump current $I_p(t)$, which can be observed at high conductivity ($\approx 30\,\mu S/cm^2$). At low conductivity ($\approx 3\,nS/cm^2$), the transient signal is expected to decay with the system time constant k_0^{-1}. The decay of the signal at higher K^+ concentrations consists of the system time constant and an additional slower process, the origin of which is unclear. This process is far too slow to be part of the enzymatic reaction cycle ($\tau > 1$ s, at saturating K^+ concentration). It could be related to high concentrations of Na^+ accumulated in the liposome or to the depletion of K^+ in the liposome.

The system time constant at $[K^+]=0$ can be clearly identified and is approximately 330 ms at 0 and at saturating K^+ concentration. At intermediate K^+ concentrations τ_0 varies between 100 and $300\,s^{-1}$. The reason for this behavior is probably an artefact of the fitting procedure. In the range of $[K^+]=1$ mM, the amplitude of τ_0 changes its sign so that the amplitude is almost zero and τ_0 cannot be resolved at these concentrations. Furthermore, in this K^+ concentration range, the additional slow process had a time constant close to the system time constant, which makes a determination of the system time constant difficult. At higher K^+ concentrations, the amplitude is restored and the system time constant can be properly observed.

4.2. The kinetic model

The K^+ dependence of the electrical pump currents generated by the NaK–ATPase are analyzed on the basis of the kinetic model introduced in Section 2. This is a minimal model and yields the same number

of time constants as found in the data. The experimental signal is characterized by two enzymatic relaxation times plus the system time constant k_0^{-1}, the size of the peak signal and the amplitude of the system time constant. These 5 experimental parameters correspond to 5 parameters of the kinetic model: k_1, k_2, k_3, sc and k_0. This ensures that the fit parameters are well determined by the experiment.

It is interesting to note that the model although consisting of three reaction steps only predicts two relaxation times. Electrical signals generated by a system behaving according to this model will always show only two relaxation times even if two or all three of the reactions are electrogenic. In fact, a third relaxation time corresponding to K^+ translocation was never experimentally observed although the rate constant of this reaction can be modified in a wide range by changing the K^+ concentration.

We assume that before starting the reaction essentially all of the enzyme is in the E_1 conformational state. In the presence of K^+, the pool of E_1 could be decreased in favor of E_2. However, this effect is counteracted by the high Na^+ concentration and the high Na^+ affinity of E_1 [33–35]. Experiments performed with fluorescein isothiocyanate labeled NaK–ATPase from pig kidney showed that at 130 mM Na^+ and 20 mM K^+ all of the enzyme is in the E_1 conformation [36].

In the kinetic model, single steps comprise several consecutive steps of the NaK–ATPase reaction cycle as outlined in Section 2. We will call the second step (k_2), in which the enzyme is phosphorylated and undergoes the $E_1P \rightarrow E_2P$ conformational transition, the Na^+ translocation. The third step of the model comprises at least the dephosphorylation reaction and the $E_2 \rightarrow E_1$ conformational transition. It will be called K^+ translocation. The rate constants determined in the model, therefore, correspond to a complex sequence of events rather than to a single reaction.

Cation binding and release steps are important in the reaction cycle of the NaK–ATPase because some of them are believed to be electrogenic [37]. They are assumed to be much faster than other reactions of the cycle [38–40]. Therefore, they are not kinetically resolvable in the measurements presented here. They rather act by influencing the rate constant and charge translocation of the neighboring rate limiting steps. In general, the rate constant and electrogenicitiy of Na^+ as well as of K^+ translocation (in the sense as defined above) will therefore depend on the cation concentrations.

The kinetic model is based on a simplified transport scheme, namely the translocation of each of the involved cations in a single step together with a fixed number of negative countercharges. Evidently, a realistic transport model has to be more complex. However, our simplified kinetic model can account for a much more complicated situation if we drop the notion that $n\_$ represents an actual number of negative charges translocated over the whole thickness of the membrane. This approach guarantees the $3/2$ stoichiometry of the transported cations. Then $(3\text{-}n\_)$ and $(2\text{-}n\_)$ are simply the charges transported during Na^+ and K^+ translocation.

4.3. K^+ Translocation is electroneutral or only weakly electrogenic

The NaK–ATPase transports Na^+ and K^+ ions with a stoichiometry close to $3/2$ [41,42]. The overall transport process is electrogenic and corresponds to one positive charge per ATP hydrolyzed [14]. To obtain insight into the transport mechanism of the ion pump, it is interesting to determine the contribution of different partial reactions to charge transport, i.e. to determine the electrogenic steps of the reaction cycle.

Electrogenic Na^+ transport has been demonstrated with a variety of techniques on different enzyme preparations (for a review, see [43,37]). The electrogenicity of the K^+ translocation step, however, is a controversial issue. From the voltage dependence of NaK–ATPase pump currents Lafaire and Schwarz [44] concluded that the transport cycle of the NaK–ATPase contains at least 2 electrogenic steps. One of these was proposed to be voltage dependent Na^+ transport and the other was voltage dependent K^+ binding [15,45]. In contrast, current voltage relationships were found that required only a single electrogenic transition [46–48] namely the Na^+ translocation.

A single voltage dependent step was also found in NaK–ATPase incorporated into liposomes. Voltage dependence was only detected during Na^+ transport,

not during K^+ transport [12,49,50]. To explain this behavior, these authors presented a transport mechanism where 2 negative protein charges are cotransported with the $3Na^+$ and $2K^+$ ions, respectively. Such a mechanism has been experimentally supported [51].

Whole cell patch clamp studies were used to investigate the voltage dependence of the NaK–ATPase [5,52]. These experiments were explained in terms of electrogenic Na^+ translocation and electroneutral K^+ translocation [13]. However, based on the same technique, but under different ionic conditions electrogenic K^+ binding in a narrow access channel was found recently [53].

Fluorescent styryl dyes were proposed to report on intramolecular charge transport in the NaK–ATPase via an electrochromic effect [54,55]. From these experiments, it was concluded that K^+ binds electrogenically via an extracellular access channel. However, the purely electrochromic mechanism of the styryl dye has been recently questioned [56,57].

In conclusion, there is apparently contradictory experimental evidence concerning the electrogenicity of the reaction steps involving K^+. To reconcile these results it has been proposed that one Na^+ ion is released and one K^+ is bound via the same narrow extracellular access channel [37]. Under saturating K^+ conditions, their charge movements cancel out resulting in an apparently electroneutral K^+ binding reaction.

In this paper, we determine the relative contributions of Na^+ and K^+ tranclocation to the charge transport of the NaK–ATPase. A quantitative treatment can be based on our kinetic model. So far, the number and position of the electrogenic steps within the model has not been discussed. Since the first step is electroneutral (ATP binding, [6]) only Na^+ translocation or K^+ translocation or both are electrogenic. In a first approach, we assumed that only Na^+ translocation is electrogenic. This model yielded good quality fits to the data as shown in Fig. 3. The parameters obtained using this procedure show a dependence on K^+ concentration as expected (Fig. 4): ATP binding (k_1) and Na^+ translocation (k_2) are independent of K^+. In contrast, K^+ translocation (k_3) depends on the K^+ concentration with a sigmoidal dependence and a half saturating value of 4.5 mM. Also consistent with the model is the independence of the scaling parameter *sc* from the K^+ concentration (Fig. 4), indicating that the amount of charge transported per turnover is constant and the same for Na^+/K^+ and Na^+/Na^+ exchange. An estimate of the acceptable electrogenicity of K^+ translocation gives the standard deviation for *sc* which is approximately 10% (Fig. 4). Taken together, these findings strongly support the concept of electrogenic Na^+ and electroneutral K^+ transport.

Now, the question arises whether the model outlined above with a single electrogenic Na^+ translocation step is unique to describe the experimental data or whether a contribution of electrogenic K^+ translocation to the net charge transport is compatible with the experimental data as well. As shown in the previous section, the fit procedure correlates five parameters of the kinetic model with five parameters of the experimental signal. Electrogenic K^+ translocation introduces an additional model parameter, the relative amount of charge transported during K^+ translocation. This parameter is taken into account by introducing the number n_- of negative charges that are cotransported with the $3Na^+$ ions and the $2K^+$ ions (Eq. (3)). The addition of n_- increases the number of fit parameters by one which makes the fit less reliable because only 5 experimental parameters are available. We, therefore, made the reasonable assumption that k_1 (ATP binding) and k_2 ($E_1ATP \rightarrow E_2P$) are both independent of the K^+ concentration. This assumption is supported by experimental evidence: Presteady state measurements of phosphorylation and phosphate release as well as electrical measurements in the absence and presence of K^+ could be analyzed using a single, K^+ independent rate constant for phosphorylation [4]. In addition, the ATP dependence of transient currents generated by the NaK–ATPase from electric eel was measured in the absence and presence of 10 mM K^+ [58]. These measurements yield similar values for the ATP affinity of the enzyme of 14 μM in the absence and 9 μM in the presence of 10 mM K^+.

Electrogenic K^+ translocation contributes most at high K^+ concentration. On the other hand, electrogenic Na^+ translocation is best measured at low K^+. Therefore, we analyzed the data at 0, 5 mM (half-saturating) and at 20 mM (saturating) K^+ concentration using a simultaneous fitting procedure. Fitting with different values of n_- we obtained $n_- =$

2.0(+0.2, −0.27) (Fig. 7). Two cotransported negative charges mean electrogenic Na^+ translocation and electroneutral K^+ translocation. The error limit allows for a range of 1.73–2.2 countercharges. At the limiting cases of 1.73 and 2.2 countercharges, the ratio of charge transported during Na^+ and K^+ translocation is $+1.27/+0.27$ and $+0.8/-0.2$, respectively. This is approximately a 20% contribution to charge transport from K^+ translocation relative to Na^+ translocation.

4.4. Electrogenic cation binding and release

So far we have analyzed the experimental results on the basis of our kinetic model which does not explicitly specify cation binding and release steps. However, since these cation binding steps are assumed to be rapid equlibria (compared to a time resolution of the measurenent of 1 ms) no additional reactions have to be introduced.

In the context of the recently introduced extracellular cation access channel (for a review, see [37]), a large part of the charge transport during Na^+ translocation is attributed to Na^+ release through a narrow access channel or ion well [59,60]. Similarly, K^+ binding is proposed to be electrogenic because K^+ has to pass the access channel on its way to the binding site [15,61]. The reactions in the access channel are believed to be extremely fast [39]. If we incorporate extracellular cation binding and release steps into our kinetic model we have to consider the following reaction sequence:

$$NaE_1ATP \overset{k_2}{\rightarrow} NaE_2P \overset{Na}{\rightleftharpoons} E_2P \overset{K}{\rightleftharpoons} KE_2P \overset{k_3}{\rightarrow} E_1. \quad (7)$$

What does that mean in terms of our simplified kinetic model Eq. (1)? We consider now only the Na^+ related part of Eq. (7). Under our conditions (130 mM Na^+, no transmembrane potential), the Na^+ equilibrium is far on the side of the unbound enzyme E_2P [5,62]. In this case, the electrogenic Na^+ release step confers its electrogenicity to the preceding reaction. Therefore, in our kinetic model (Eq. (1)), the reaction characterized by k_2 maintains its rate constant but comprises the charge transport of two reactions: $NaE_1ATP \rightarrow NaE_2P$ and $NaE_2P \rightleftharpoons E_2P$.

In the next step, we add the K^+ related reactions of Eq. (7). It is assumed that of the two reactions only K^+ binding is electrogenic [37]. Depending on K^+ concentration, the K^+ binding step confers its electrogenicty either to the preceding $E_1ATP \rightarrow E_2P$ or to the subsequent $KE_2P \rightarrow E_1$ reactions. At low K^+ concentration this results in an apparently electrogenic $E_2P \rightarrow E_1$ step but with a very small rate constant (see Eq. (1)). In contrast, at saturating K^+ concentration all the electrogenicity goes to the $E_1ATP \rightarrow E_2P$ step. Since K^+ binding means transport of positive charge to the opposite direction than in the Na^+ related steps this effect reduces the apparent electrogenicity of $E_1ATP \rightarrow E_2P$.

Taken together the following behavior of the parameters of our kinetic model is predicted: (1) Electrogenic K^+ translocation ($E_2P \rightarrow E_1$, k_3) at nonsaturating K^+ concentrations. This requires a number of cotransported negative charges of $n_- < 2$; (2) Electroneutral K^+ translocation at saturating $[K^+]$ ($n = 2$); (3) A reduction of electrogenicity of Na^+ translocation with increasing K^+ concentration. Together, these predictions imply an increase of n_- with increasing K^+ concentration.

The conditions (2) and (3) are clearly not in agreement with our experimental data since they require a different value of n_- at different K^+ concentrations. In contrast, the data can very well be fitted with a constant $n_- = 2$ independent of the K^+ concentration (Fig. 4(A) and (B)). An error analysis is difficult in this case since the procedure of Fig. 7 is based on a K^+ independent n_-. Therefore, we will use the value determined there ($n_- = 1.7$–2.2) as a reasonable estimate for a possible variation of n_-. Assuming an electrogenic cation binding mechanism as described above, the variation of n_- from 0 to saturating K^+ concentration gives the contribution of cation binding to electrogenic transport. Our data therefore give an upper limit of $0.5/2.2 \approx 20\%$ charge transport from electrogenic K^+ binding relative to total Na^+ translocation (from the cytoplasmic to the extracellular surface of the protein).

From the arguments given above it becomes clear, that a transport model with electrogenic K^+ binding and an electroneutral $E_2P \rightarrow E_1$ transition can solve some of the apparent contradictions found in the literature. However, only a moderate fraction of 20% of the charge transported during Na^+ translocation can be assigned to electrogenic K^+ binding.

4.5. The K^+ affinity of the NaK–ATPase and the $E_2 \rightarrow E_1$ transition

The evaluation of the experiments revealed that k_3 increased with increasing K^+ concentration, whereas k_1 and k_2 remained constant. This clearly confirms $E_2P \rightarrow E_1$ to be a $[K^+]$ controlled process. For the analysis of the electrical current obtained at different K^+ concentrations, we used a sequential two-step binding model. The microscopic dissociation constant K_3 for the reaction $E_2P \rightarrow E_1$ is 1.9 mM (average value of K_3 from Table 1) and the half saturating concentration $K_{3,0.5}$ is 4.5 mM. Further, the Na^+ concentration does not influence the extracellular affinity for K^+ up to a Na^+ concentration of 130 mM (Table 1).

Additional information comes from stationary experiments. The half saturating concentration in this case was 0.95 mM. This can be compared with $K_{3,0.5}$ as determined from the transient currents. For each K^+ concentration of the nonstationary experiments the turnover k_t of the NaK–ATPase can be calculated by simply adding the reciprocal reaction rate constants: $1/k_t = 1/k_1 + 1/k_2 + 1/k_3$. In Fig. 8 the turnover rate (calculated from the transient currents of Experiment 1) over the K^+ concentration is shown. The fit with Eq. (5) gives an apparent half saturating concentration $K_{t,0.5}$ of 1.25 mM. Since the turnover rate is directly proportional to the stationary current, the nonstationary experiments are in good agreement with the stationary experiments ($K_{t,0.5} = 0.95$ mM).

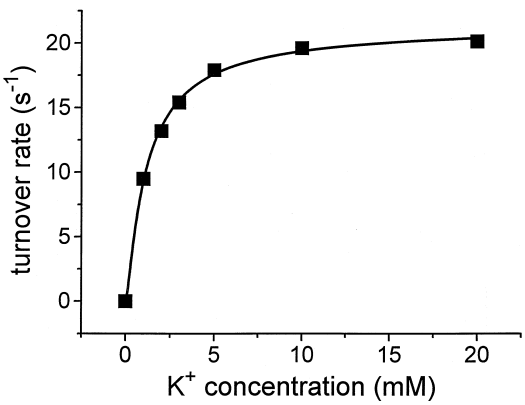

Fig. 8. Calculated turnover rates at different K^+ concentrations (data from Experiment 1). Apparent dissociation constant K_t = 0.52 mM, half saturating value $K_{t,0.5} = 1.25$ mM.

The agreement gives additional support to the kinetic model and to the analysis of the transient currents.

The half saturating concentration for the K^+ binding under steady state conditions $K_{t,0.5} = 0.95$ mM is in good agreement with values found in literature, ranging from 0.46 to 1.5 mM [15,63–66]. Bühler and Apell [8] determined an apparent half saturating value of $K_{0.5} = 0.192$ mM. The reason for the rather large discrepancy to our data is not known.

As a last point, the maximum values of the reaction rate constant k_3 as shown in Table 1 shall be discussed. $k_{3,max}$ varies from 95 s^{-1} to 125 s^{-1} at saturating K^+ concentrations. Here we have to consider the two processes that are summarized in k_3, the dephosphorylation and the $E_2 \rightarrow E_1$ conformational transition. Reaction rate constants for the dephosphorylation vary from 300 s^{-1} [16] to 10^5 s^{-1} [10]. Data obtained with NaK–ATPase from shark rectal gland reconstituted into liposomes give a value of 4.4 s^{-1} at 0°C and 14.4 s^{-1} at 10°C [31,32] corresponding to approximately 75 s^{-1} at 24°C when corrected for the temperature difference.

Karlish [67] estimated the reaction rate constant $E_2 \rightarrow E_1$ to be approximately 18 s^{-1} at 100 μM ATP. Kane [68] found at saturating ATP concentrations a value of 28 s^{-1}. In our experiments, ca. 60 μM ATP are released after each light flash. On the other hand, caged ATP is present at a concentration of 300 μM and the $E_2 \rightarrow E_1$ transition could be accelerated by caged ATP in much the same way as nonhydrolyzable ATP analogues accelerate this reaction. Taking together the published rate constants for the dephosphorylation $E_2P \rightarrow E_2$ and $E_2 \rightarrow E_1$ conformational transition we can say that most probably the conformational transition limits our measured rate constant k_3 of 95–125 s^{-1}. The large differences found in the literature for the rate constant of the dephosphorylation step make a clearcut decision difficult. However, this reaction could also contribute to rate limitation of k_3.

5. Conclusions

The K^+ translocation reaction of the NaK–ATPase is proposed to be electroneutral. The data are best approximated using a kinetic model where 2 negative

countercharges are cotransported with the $3Na^+$ and the $2K^+$ ions. Error analysis gives an upper limit of 20% charge transport during K^+ translocation relative to Na^+ translocation. Our data do not explicitly support electrogenic K^+ binding in an extracellular access channel. However, approximately 20% charge translocation during electrogenic K^+ binding compared to Na^+ translocation are compatible with the experimental uncertainty.

For the K^+ dependence of the reaction $E_2P \rightarrow E_1$ and of the turnover rate, we obtain half saturating concentrations of approximately 4.5 and 1 mM, respectively. In a two-step K^+ binding model with identical binding sites followed by the reaction $E_2P \rightarrow E_1$ this corresponds to a microscopic dissociation constant of approximately 1.9 mM.

Acknowledgements

We thank B. Kelety for advice on the reconstitution procedure. E. Bamberg, R. Clarke, J. Froehlich, E. Grell, D. Kane, J. Rettinger, W. Schwarz, and L. Vasilets are gratefully acknowledged for useful discussions and critical suggestions.

Appendix A. Kinetic model

The kinetic model is a simplified Albers–Post mechanism, in which the back reactions are neglected:

$$E_1 \overset{k_1}{\rightarrow} E_1ATP \overset{k_2}{\rightarrow} E_2P \overset{k_3}{\rightarrow} E_1. \tag{8}$$

Several steps of the Albers-Post cycle are summarized in one reaction rate constant: k_1 represents the binding of ATP and the exchange with caged ATP, k_2 the phosphorylation and the electrogenic step ($E_1P \rightarrow E_2P$), and k_3 the dephosphorylation and the conformational transition $E_2 \rightarrow E_1$. Further, let y_1 be the number of enzyme molecules in conformation E_1, y_2 the number of enzyme molecules in conformation E_1ATP and y_3 the number of enzyme molecules in conformation E_2P.

Assuming the electrogenic step is $E_1P \rightarrow E_2P$, the generated pump current is:

$$I_p(t) = \text{const}\, k_2\, y_2(t). \tag{9}$$

The kinetic model yields a homogeneous linear system consisting of three coupled first order differential equations:

$$\frac{dy_1}{dt} = k_3 y_3 - k_1 y_1, \tag{10}$$

$$\frac{dy_2}{dt} = k_1 y_1 - k_2 y_2, \tag{11}$$

$$\frac{dy_3}{dt} = k_2 y_2 - k_3 y_3. \tag{12}$$

Let the initial values be $y_1(t=0) = 1$, $y_2(t=0) = 0$, and $y_3(t=0) = 0$.

The characteristic equation yields the following eigenvalues λ_i:

$$\lambda_1 = 0, \tag{13}$$

$$\lambda_2 = \frac{-(k_1 + k_2 + k_3)}{2} + \frac{\sqrt{d}}{2}, \tag{14}$$

$$\lambda_3 = \frac{-(k_2 + k_2 + k_3)}{2} - \frac{\sqrt{d}}{2}, \tag{15}$$

with the discriminant

$$d = k_1^2 + k_2^2 + k_3^2 - 2k_1k_2 - 2k_1k_3 - 2k_2k_3. \tag{16}$$

Since the discriminant d can be positive or negative, there are real as well as complex solutions of the characteristic equation. Therefore, we have to distinguish three cases.

Case 1: $d > 0$

If $d > 0$ and with the above initial conditions the solution is:

$$y_2(t) = a_1 + a_2 e^{\lambda_2 t} + a_3 e^{\lambda_3 t}. \tag{17}$$

The amplitudes are:

$$a_1 = \frac{k_1k_3}{k_1k_2 + k_1k_3 + k_2k_3}, \tag{18}$$

$$a_2 = \frac{k_1\left(-\sqrt{d} + k_1 + k_2 - k_3\right)}{\sqrt{d}\left(-\sqrt{d} + k_1 + k_2 + k_3\right)} \tag{19}$$

$$a_3 = \frac{k_1\left(-\sqrt{d} - k_1 - k_2 + k_3\right)}{\sqrt{d}\left(\sqrt{d} + k_1 + k_2 + k_3\right)}. \tag{20}$$

Case 2: $d = 0$

Since case 2 ($d=0$) is only occurring in two points and follows as a limit value from case 1 or 3, it is not necessary to discuss this case separately.

Case 3: $d<0$

In the case $d<0$, we get a complex solution of the characteristic equation so that $y_2(t)$ is

$$y_2(t) = a_1 + e^{\omega_1 t}\left[b_1 \sin(\omega_2 t) + b_2 \cos(\omega_2 t)\right] \quad (21)$$

with

$$\omega_1 = -\frac{k_1+k_2+k_3}{2}, \quad (22)$$

$$\omega_2 = \frac{\sqrt{|d|}}{2} \quad (23)$$

$$b_1 = 2k_1 \frac{k_1^2 + 2k_1k_2 + k_2^2 - k_3^2 + d}{\sqrt{d}\left((k_1+k_2+k_3)^2 + d\right)}, \quad (24)$$

$$b_2 = -\frac{4k_1k_3}{(k_1+k_2+k_3)^2 + d}. \quad (25)$$

Appendix B. Electrical properties of the system and calculation of the measured current

In Fig. 1, the equivalent circuit for the system proteoliposomes adsorbed to a planar lipid bilayer is shown. It is evident, that the capacitive coupling of the protein to the measuring circuit has to be taken into account.

The measured current $I(t)$ can be calculated from the pump current $I_p(t)$ as described by Borlinghaus [21]. This yields for the measured current:

Case 1: $d>0$

$$\frac{I(t)}{\text{const}} = \left(k_2 a_3 - \frac{k_2 k_0 a_3}{\lambda_3 + k_0}\right) e^{\lambda_3 t} + \left(k_2 a_2 - \frac{k_2 k_0 a_2}{\lambda_2 + k_0}\right) e^{\lambda_2 t} + \left(k_2 a_1 + \frac{k_2 k_0 a_2}{\lambda_2 + k_0} + \frac{k_2 k_0 a_3}{\lambda_3 + k_0}\right) e^{-k_0 t}. \quad (26)$$

Case 3: $d<0$

$$\frac{I(t)}{\text{const}} = \left(k_2 a_1 - \frac{k_0 k_2 b_1 \omega_2}{(\omega_1 + k_0)^2 + \omega_2^2} + \frac{k_0 k_2 b_2 (\omega_1 + k_0)}{(\omega_1 + k_0)^2 + \omega_2^2}\right) e^{-k_0 t} + e^{\omega_1 t}\left[\left(k_2 b_1 - \frac{k_0 k_2 b_1 \omega_2}{(\omega_1 + k_0)^2 + \omega_2^2} - \frac{k_0 k_2 b_2 \omega_2}{(\omega_1 + k_0)^2 + \omega_2^2}\right)\sin(\omega_2 t) + \left(k_2 b_2 - \frac{k_0 k_2 b_1 (\omega_1 + k_0)}{(\omega_1 + k_0)^2 + \omega_2^2} - \frac{k_0 k_2 b_2 (\omega_1 + k_0)}{(\omega_1 + k_0)^2 + \omega_2^2}\right)\cos(\omega_2 t)\right]. \quad (27)$$

Appendix C. Fitting procedures

C.1. Fit with differential equations

For the differential equation fitting method, the differential Eqs. (10)–(12) were numerically solved with the initial conditions $y_1(0)=1$, $y_2(0)=0$, $y_3(0)=0$ and $u_m(0)=0$. The current was calculated according to

$$\frac{du_m}{dt} = k_2 y_2 - k_0 u_m, \quad (28)$$

$$I = sc(k_2 y_2 - k_0 u_m), \quad (29)$$

assuming only electrogenic Na^+ transport.

C.2. Fit with analytical solutions of the differential equations

From the cases $d>0$ and $d<0$ two different fitting functions are derived:

$d>0$:

$$I_1(t) = \sum_{i=1}^{3} A_i e^{-\frac{t}{\tau_i}} \quad (30)$$

with $\tau_1^{-1} = -\lambda_3$, $\tau_2^{-1} = -\lambda_2$ and $\tau_3^{-1} = k_0$.

$d < 0$:

$$I_2(t) = e^{\omega_1 t}\left(B_1 \sin(\omega_2 t) + B_2 \cos(\omega_2 t)\right) + A_0 e^{k_0 t} \quad (31)$$

with $\omega_1 < 0$.

References

[1] P. Läuger, Electrogenic Ion Pumps, Sunderland, 1991, pp. 168–224.
[2] S. Mårdh, Ö. Zetterquist, Biochim. Biophys. Acta 350 (1974) 473–483.
[3] J.P. Froehlich, R.W. Albers, G.J. Koval, R. Goebel, M. Berman, J. Biol. Chem. 251 (1976) 2186–2188.
[4] K. Fendler, S. Jaruschewski, J.P. Froehlich, W. Albers, E. Bamberg, in: E. Bamberg, W. Schoner (Eds.), The Sodium Pump, Steinkopf, Darmstadt, Springer, New York, 1994, pp. 495–506.
[5] M. Nakao, D.C. Gadsby, Nature 323 (1986) 628–630.
[6] K. Fendler, E. Grell, E. Bamberg, FEBS Lett. 224 (1987) 83–88.
[7] H.-J. Apell, R. Borlinghaus, P. Läuger, J. Membr. Biol. 97 (1987) 179–191.
[8] R. Bühler, H.J. Apell, J. Membr. Biol. 145 (1995) 165–173.
[9] D.C. Gadsby, R.F. Rakowski, P. DeWeer, Science 260 (1993) 100–103.
[10] S. Heyse, I. Wuddel, H.J. Apell, W. Stürmer, J. Gen. Physiol. 104 (1994) 197–240.
[11] J. Pintschovius, unpublished results.
[12] R. Goldshleger, S.J.D. Karlish, A. Rephaeli, J. Physiol. 387 (1987) 331–355.
[13] A. Bahinski, M. Nakao, D.C. Gadsby, Proc. Natl. Acad. Sci. U.S.A. 85 (1988) 3412–3416.
[14] H.-J. Apell, J. Membr. Biol. 110 (1989) 103–114.
[15] R.F. Rakowski, L.A. Vasilets, J. LaTona, W. Schwarz, J. Membr. Biol. 121 (1991) 177–187.
[16] A.S. Hobbs, R.W. Albers, J.P. Froehlich, J. Biol. Chem. 255 (1980) 3395–3402.
[17] K. Fendler, E. Grell, M. Haubs, E. Bamberg, EMBO J. 4 (1985) 3079–3085.
[18] M. Esmann, J.C. Skou, C. Christiansen, Biochim. Biophys. Acta 567 (1979) 410–420.
[19] F. Cornelius, J.C. Skou, Biochim. Biophys. Acta 772 (1984) 357–373.
[20] P.W. Holloway, Anal. Biochem. 53 (1973) 304–308.
[21] R. Borlinghaus, H.J. Apell, P. Läuger, J. Membr. Biol. 97 (1987) 161–178.
[22] K. Barabas, L. Keszthelyi, Biochim. Biophys. Acta Acad. Sci. Hungar. 19 (1984) 305–309.
[23] J.W. Walker, G.P. Reid, J.A. McCray, D.R. Trentham, JACS 110 (1988) 7170–7177.
[24] F. Cornelius, Biochim. Biophys. Acta 1071 (1991) 19–66.
[25] H.J. Apell, B. Bersch, Biochim. Biophys. Acta 903 (1987) 480–494.
[26] R.J. Clarke, H.J. Apell, P. Läuger, Biochim. Biophys. Acta 981 (1989) 326–336.
[27] F. Cornelius, Biochem. Biophys. Res. Commun. 160 (1989) 801–807.
[28] K. Fendler, S. Jaruschewski, A. Hobbs, W. Albers, J.P. Froehlich, J. Gen. Physiol. 102 (1993) 631–666.
[29] P. Läuger, H.J. Apell, Eur. Biophys. J. 13 (1986) 309–321.
[30] P.R. Bevington, Data Reduction and Error Analysis for the Physical Sciences, McGraw Hill, New York, 1969, p. 243.
[31] F. Cornelius, Biochim. Biophys. Acta 1235 (1995) 197–204.
[32] F. Cornelius, Biochim. Biophys. Acta 1235 (1995) 205–212.
[33] F. Cornelius, J.C. Skou, Biochim. Biophys. Acta 904 (1987) 353–364.
[34] F. Cornelius, Biochim. Biophys. Acta 1108 (1992) 190–200.
[35] S.J.D. Karlish, J. Bioenerg. Biomembr. 12 (1980) 111–136.
[36] R. Warmuth, E. Grell, unpublished results.
[37] R.F. Rakowski, D.C. Gadsby, P. De Weer, J. Membr. Biol. 155 (1997) 105–112.
[38] I. Wuddel, H.J. Apell, Biophys. J. 69 (1995) 909–921.
[39] D. Hilgemann, Science 263 (1994) 1429–1432.
[40] J. Wagg, M. Holmgren, D.C. Gadsby, F. Benzanilla, R.F. Rakowski, P. De Weer, J. Gen. Physiol. 108 (1996) 30a.
[41] L.E. Hokin, J.F. Dixon, in: S. Fleischer, B. Fleischer (Eds.), Methods in Enzymology, vol. 156, Academic Press, New York, 1988, pp. 141–155.
[42] S.J.D. Karlish, U. Pick, J. Physiol. 312 (1981) 505–529.
[43] F. Cornelius, Biomembr. 5 (1996) 133–184.
[44] A.V. Lafaire, W. Schwarz, J. Membr. Biol. 91 (1986) 43–51.
[45] A. Sagar, R.F. Rakowski, J. Gen. Physiol. 103 (1994) 869–894.
[46] D.C. Gadsby, J. Kimura, M. Nakao, Nature 315 (1985) 63–65.
[47] D.C. Gadsby, M. Nakao, J. Gen. Physiol. 94 (1989) 511–537.
[48] M.M. Wu, M.M. Civan, J. Membr. Biol. 121 (1991) 23–36.
[49] A. Rephaeli, D.E. Richards, S.J.D. Karlish, J. Biol. Chem. 261 (1986) 6248–6254.
[50] A. Rephaeli, D.E. Richards, S.J.D. Karlish, J. Biol. Chem. 261 (1986) 12437–12440.
[51] F. Cornelius, Biochim. Biophys. Acta 1235 (1995) 183–196.
[52] H.G. Glitsch, T. Krahn, H. Pusch, Pflügers Archiv 414 (1989) 52–58.
[53] R.D. Peluffo, J.R. Berlin, Biophys. J. 70 (1996) A18, (abstract).
[54] R. Bühler, W. Stürmer, H.J. Apell, P. Läuger, J. Membr. Biol. 121 (1991) 141–161.
[55] W. Stürmer, R. Bühler, H.J. Apell, P. Läuger, J. Membr. Biol. 121 (1991) 163–176.
[56] J. Frank, A. Zouni, A. van Hoek, A.J.W.G. Visser, R.J. Clarke, Biochim. Biophys. Acta 1280 (1996) 51–64.
[57] N.U. Fedosova, F. Cornelius, I. Klodos, Biochemistry 34 (1995) 16806–16814.
[58] S. Jaruschewski, Ph.D. thesis, University Frankfurt, 1995.

[59] P. Läuger, Biochim. Biophys. Acta 552 (1979) 143–161.
[60] C. Tanford, Proc. Natl. Acad. Sci. U.S.A. 80 (1983) 3701–3705.
[61] L.A. Vasilets, T. Ohta, S. Noguchi, M. Kawamura, W. Schwarz, Eur. Biophys. J. 21 (1993) 433–443.
[62] T. Friedrich, E. Bamberg, G. Nagel, Biophys. J. 71 (1996) 2486–2500.
[63] G. Nagel, K. Fendler, E. Grell, E. Bamberg, Biochim. Biophys. Acta 901 (1987) 239–249.
[64] C. Gache, B. Rossi, F.A. Leone, M. Lazdunsk, in: J.C. Skou, J.G. Norby (Eds.), NaK–ATPase Structure and Kinetics, Academic Press, London, 1979, pp. 301–314.
[65] D.C. Gadsby, Proc. Natl. Acad. Sci. U.S.A. 77 (1980) 4035–4039.
[66] M. Nakao, C. Gadsby, J. Gen. Physiol. 94 (1989) 539–565.
[67] S.J.D. Karlish, D.W. Yates, I.M. Glynn, Biochim. Biophys. Acta 525 (1978) 252–264.
[68] D.J. Kane, K. Fendler, E. Grell, E. Bamberg, K. Taniguchi, J.P. Froehlich, R.J. Clarke, Biochemistry 36 (1997) 13406–13420.